Chinese Journal of Natural Medicines

Brevilin A induces mitochondrial dysfunction and endoplasmic reticulum stress in breast cancer through WWP2-mediated KLF5 degradation

Yuan Si, Wenkang Peng, Ling Liu, Miao Tan, Sicheng Wang, Chengling Zheng, Peng Peng, Qiang Xia, Kainan Zheng, Xuewen Liu, Ying Liu, Yan Tan

Citation: Yuan Si, Wenkang Peng, Ling Liu, Miao Tan, Sicheng Wang, Chengling Zheng, Peng Peng, Qiang Xia, Kainan Zheng, Xuewen Liu, Ying Liu, Yan Tan, Brevilin A induces mitochondrial dysfunction and endoplasmic reticulum stress in breast cancer through WWP2-mediated KLF5 degradation, Chinese Journal of Natural Medicines, 2026, 24(11), 1379-1391. doi: 10.1016/S1875-5364(26)61227-7.

View online: https://doi.org/10.1016/S1875-5364(26)61227-7

Related articles that may interest you

Therapeutic potential of alkaloid extract from Codonopsis Radix in alleviating hepatic lipid accumulation: insights into mitochondrial energy metabolism and endoplasmic reticulum stress regulation in NAFLD mice

Chinese Journal of Natural Medicines. 2023, 21(6), 411-422 https://doi.org/10.1016/S1875-5364(23)60403-0

Polyphyllin I promotes cell death *via* suppressing UPR-mediated CHOP ubiquitination and degradation in non-small cell lung cancer

Chinese Journal of Natural Medicines. 2021, 19(4), 255-266 https://doi.org/10.1016/S1875-5364(21)60027-4

Oroxyloside protects against dextran sulfate sodium-induced colitis by inhibiting ER stress *via* PPAR γ activation

Chinese Journal of Natural Medicines. 2024, 22(4), 307-317 https://doi.org/10.1016/S1875-5364(24)60615-1

Design, synthesis, and biological evaluation of novel chrysin derivatives as poly(ADP-ribose) polymerase 1 (PARP1) inhibitors for the treatment of breast cancer

Chinese Journal of Natural Medicines. 2024, 22(5), 455-465 https://doi.org/10.1016/S1875-5364(24)60642-4

Potentilla anserina polysaccharide alleviates cadmium-induced oxidative stress and apoptosis of H9c2 cells by regulating the MG53-mediated RISK pathway

Chinese Journal of Natural Medicines. 2023, 21(4), 279-291 https://doi.org/10.1016/S1875-5364(23)60436-4

Ziyuglycoside II inhibits the growth of digestive system cancer cells through multiple mechanisms

Chinese Journal of Natural Medicines. 2021, 19(5), 351-363 https://doi.org/10.1016/S1875-5364(21)60033-X

Wechat

Chinese Journal of Natural Medicines 24 (2026) 1379-1391

Contents lists available at ScienceDirect

Chinese Journal of Natural Medicines

journal homepage: www.cjnmcpu.com/



Original article

Brevilin A induces mitochondrial dysfunction and endoplasmic reticulum stress in breast cancer through WWP2-mediated KLF5 degradation

Yuan Si[a,b,c,Δ*], Wenkang Peng[a,c,Δ], Ling Liu[a,Δ], Miao Tan[a], Sicheng Wang[a], Chengling Zheng[a], Peng Peng[a], Qiang Xia[a], Kainan Zheng[a], Xuewen Liu[a,b], Ying Liu[a,b,*], Yan Tan[a,b,*]

[a] *School of Basic Medical Sciences, Hubei University of Medicine, Shiyan 442000, China*
[b] *Hubei Key Laboratory of Wudang Local Chinese Medicine Research, Hubei University of Medicine, Shiyan 442000, China*
[c] *Hubei Key Laboratory of Embryonic Stem Cell Research, Hubei University of Medicine, Shiyan 442000, China*

ARTICLE INFO

Article history:
Received 12 March 2026
Revised 16 July 2026
Accepted 25 August 2026
Available online 20 November 2026

Keywords:
Brevilin A
Breast cancer
KLF5
Mitochondrial dysfunction
Endoplasmic reticulum stress
WWP2

ABSTRACT

Breast cancer (BC) remains a significant challenge to women's health, and identifying effective molecular targets is crucial for therapeutic advancement. Krüppel-like factor 5 (KLF5), an oncogenic transcription factor, is highly expressed in BC, yet its development as a therapeutic target has been hindered by its intrinsically disordered structure. In this study, we identified Brevilin A (BrA), a natural sesquiterpenoid from *Centipeda minima*, as a potent KLF5 degrader. We demonstrated that BrA directly binds to KLF5 and promotes its ubiquitin-mediated degradation through the E3 ligase WWP2. BrA significantly inhibited BC cell proliferation and induced severe mitochondrial dysfunction and endoplasmic reticulum (ER) stress, as evidenced by reduced mitochondrial respiration and activation of the PERK-EIF2α pathway. Mechanistically, BrA enhanced the recruitment of WWP2 to KLF5, leading to its polyubiquitination and subsequent proteasomal degradation. KLF5 overexpression effectively rescued the mitochondrial and ER homeostasis disrupted by BrA, whereas KLF5 knockdown rendered cells insensitive to BrA-induced cytotoxicity. *In vivo* studies using zebrafish and nude mouse xenograft models confirmed that BrA suppressed tumor growth by downregulating KLF5 and its downstream metabolic effectors. Collectively, our findings reveal that BrA exerts antitumor effects by promoting WWP2-mediated ubiquitination and degradation of KLF5, thereby disrupting mitochondrial and ER integrity, highlighting its potential as a natural lead compound for BC treatment.

1. Introduction

Breast cancer (BC) remains the most prevalent malignancy and a leading cause of cancer-related mortality among women worldwide [1]. Despite the diversification of treatment strategies and the advancement of precision medicine [2], the inherent metabolic plasticity and stress adaptation of BC cells continue to drive therapeutic resistance. Consequently, identifying novel molecular targets that govern these adaptive processes is essential for developing more effective targeted therapies.

Krüppel-like factor 5 (KLF5), a zinc-finger transcription factor, has emerged as a central oncogenic driver in cancer [3-7]. It orchestrates transcriptional programs that promote cell cycle progression, epithelial-mesenchymal transition, and apoptosis resistance through targets such as MYC and CCND1 [8]. Crucially, KLF5 acts as a pivotal metabolic rheostat in BC [9-11]. Emerging evidence indicates that KLF5 maintains mitochondrial integrity and bioenergetics by transcriptionally regulating key factors such as MFN1 and eIF5A [12-15]. Disruption of KLF5-mediated transcriptional control leads to mitochondrial fragmentation, impaired oxidative phosphorylation, and excessive reactive oxygen species (ROS) accumulation [16, 17]. This mitochondrial dysfunction, in turn, triggers a reciprocal stress response in the endoplasmic reticulum (ER). The resulting mitochondrial-ER crosstalk, characterized by Ca^{2+} imbalance and persistent activation of the unfolded protein response (UPR), serves as a critical determinant of tumor cell fate—shifting the balance from metabolic adaptation to apoptosis [18-20]. Thus, targeting the KLF5-mediated ER-mitochondrial axis represents a compelling strategy to overcome the metabolic resilience of BC.

Given its oncogenic significance, the post-translational regulation of KLF5 protein stability is a highly controlled process, primarily governed by the ubiquitin-proteasome system (UPS) [21, 22]. Several E3 ligases, including FBXW7, SMURF2, TRIM25, and WWP1, have been reported to regulate KLF5 stability through ubiquitin-mediated proteasomal degradation [23-26]. Dysregulation of this process can lead to aberrant accumulation of KLF5, thereby promoting tumor progression. WW domain-containing E3 ubiquitin protein ligase 2 (WWP2), a member of the HECT-domain E3 ligase family, has been implicated in controlling protein stability across multiple cancer types [27, 28]. However, whether WWP2 directly regulates KLF5 ubiquitination and degradation remains to be elucidated.

* Corresponding author.
E-mail addresses: siyuan138@126.com (Y. Si); ying_liu1002@163.com (Y. Liu); tanyan-1@163.com (Y. Tan)
Δ These authors contributed equally to this work.

https://doi.org/10.1016/S1875-5364(26)61227-7
Copyright © 2026, China Pharmaceutical University. Published by Elsevier B.V. All rights reserved.

Brevilin A (BrA), one of the major sesquiterpene lactones isolated from *Centipeda minima* with an average content of approximately 1.88 mg·g^{-1} [29], has demonstrated potent anti-tumor activities across various cancers [30]. While BrA is known to inhibit BC cell proliferation and induce apoptosis [31, 32], its precise molecular targets and its role in regulating tumor metabolism remain largely uncharacterized. In this study, we provide evidence that BrA promotes WWP2-mediated ubiquitination and degradation of KLF5. This downregulation subsequently collapses ER-mitochondrial homeostasis, leading to metabolic failure in BC cells. Our findings thus delineate a novel mechanism by which BrA exerts antitumor effects against BC.

2. Materials and methods

2.1. Reagents

BrA with a purity of up to 97% was purchased from Nature-Standard Co., Ltd. (Shanghai, China). PS-341, MG-132, Mito-TEMPO, and cisplatin (DDP) were purchased from MCE.

2.2. Cell culture

The human BC cell lines MCF7, MDA-MB-231, and BT474 were purchased from American Type Culture Collection (ATCC, USA). The cells were cultured in DMEM (Gibco, USA) with 10% FBS (#SA311, CellMax, Beijing, China) and incubated in 5% CO_2 at 37° C.

2.3. Cytotoxicity assay, cell viability, and colony formation assay

Cell cytotoxicity and viability were evaluated by the CCK-8 assay, RTCA, and colony formation assay as previously described [33].

2.4. High-content analysis

An Operetta CLS high-content analysis system (PerkinElmer, Germany) was used to examine the morphology of cells. Cells were seeded into 96-well plates, and cell area and roundness were monitored in real time for 60 h [34].

2.5. RNA-seq analysis

BT474 cells were treated with BrA for 24 h. Total RNA was isolated using TRIzol reagent (Invitrogen, USA) according to the manufacturer's instructions. RNA-seq was conducted by Novogene Co., Ltd. (Shanghai, China). The raw reads were aligned to the GRCh38 human reference genome using HISAT2, and gene-level counts were quantified with featureCounts. Differential gene expression analysis was performed using the DESeq2 package in R. Significantly enriched KEGG pathways were identified with the clusterProfiler R package.

2.6. Mitochondrial permeability transition pore (mPTP) opening assay

The cells were incubated with calcein AM (Beyotime, China) according to the manufacturer's instructions and then subjected to flow cytometry analysis [27].

2.7. Measurement of mitochondrial reactive oxygen species (mitoROS)

The cells were incubated with MitoSOX^{TM} Red FM (Thermo Fisher Scientific, USA) according to the manufacturer's instructions and then subjected to flow cytometry analysis.

2.8. Live cell imaging

Cells were seeded in 35 mm glass-bottom dishes (Jet Biofil, China). For mitochondrial morphology analysis, cells were transfected with Mito-DsRed plasmid for 6 h, treated with BrA for 24 h, and imaged by confocal microscopy.

For ER-mitochondria interaction analysis, cells were transfected with EGFP-ER plasmid for 6 h, treated with BrA for 24 h, stained with Mito-Tracker Red (Beyotime, China), and subsequently imaged using a confocal laser scanning microscope. ER-mitochondria colocalization was analyzed using ImageJ software. (Olympus, FV3000RS) [35].

2.9. Cellular oxygen consumption rate (OCR) assay

Cellular OCR was measured on a Seahorse XFe24 Analyzer (Agilent Technologies, USA). Briefly, cells (5000 cells/well) were incubated in assay medium (supplemented with 1 mmol·L^{-1} sodium pyruvate, 2 mmol·L^{-1} glutamine, and 10 mmol·L^{-1} glucose) for 1 h, then OCR was measured following the sequential addition of oligomycin (1.5 μmol·L^{-1}), FCCP (2 μmol·L^{-1}), and rotenone/antimycin A (0.5 μmol·L^{-1}). Data were normalized to cell number per well [36].

2.10. Mitochondrial DNA (mtDNA) quantification

Total DNA was extracted from cells using a Universal Genomic DNA Kit (TIANGEN, China). qPCR experiments were performed using mtDNA primers. The mtDNA primers sequences are listed in Table 1.

Table 1 Primer sequences for qPCR.

Gene	Primer sequences (5'-3')
KLF5	F: CCTGGTCCAGACAAGATGTGA
	R: GAACTGGTCTACGACTGAGGC
MT-ND1	F: ACGCCATAAAACTCTTCACCAAAG
	R: GGGTTCATAGTAGAAGAGCGATGG
MT-ND4	F: ACCTTGGCTATCATCACCCGAT
	R: AGTGCGATGAGTAGGGGAAGG
MT-CO1	F: GATTTTTCGGTCACCCTGAAG
	R: CTCAGACCATACCTATGTATC
α-tubulin	F: TCGATATTGAGCGTCCAACCT
	R: CAAAGGCACGTTTGGCATACA

F, forward; R, reverse.

2.11. Western blot

Western blot was conducted as previously described [37]. The primary antibodies used were anti-phospho-DRP1 (S616) (Cat# 4494), anti-DRP1 (Cat# 5391), anti-Bip (Cat# 3177), anti-ATF4 (Cat# 11815), anti-phospho-PERK (Thr980) (Cat# 3179), anti-PERK (Cat# 3192), anti-phospho-EIF2α (Ser51) (Cat# 3398), anti-EIF2α (Cat# 5324), anti-KLF5 (Cat# 51586), anti-Myc (Cat# 3739,), anti-Flag (Cat# 14793), and anti-HA (Cat# 3724) (Cell Signaling Technology, USA); anti-MFN1/2 (Cat# ab57602)(Abcam, USA); and anti-WWP2 (Cat# 67274-1-Ig), and anti-α-tubulin (Cat# 11224-1-AP) (Proteintech Group, USA).

2.12. Quantification of ER stress

The ER stress level was quantified by flow cytometry using

ER-Tracker Red. In brief, cells were seeded in a 6-well plate at a density of 5 × 10^5 cells/well and treated with BrA for 24 h. Following treatment, the cells were incubated with ER-Tracker Red dye (Beyotime, China) for 15 min. The relative median fluorescence intensity (MFI) associated with the ER was then measured using a flow cytometer.

2.13. DARTS-MS

For the drug affinity responsive target stability (DARTS) assay, cell lysates were incubated with BrA or DMSO for 3 h at room temperature. Following this, limited proteolysis was carried out using pronase (Sigma-Aldrich, USA) for 3 h. The proteolytic fragments were then resolved by SDS-PAGE and stained with Coomassie Brilliant Blue. Potential target proteins protected by BrA from digestion were identified by subsequent mass spectrometry (Bioprofile, Shanghai, China).

2.14. Plasmid constructs and cell transfection

The full-length *KLF5* coding sequence was cloned into pcDNA3.1 vectors with HA or EGFP tags, and its deletion mutants into pcDNA3.1-EGFP. *CCT3*, *PDIA3*, *RTCB*, *PHGDH*, *HMGCS1*, *SHMT2*, and *DNAJC7* were cloned into pcDNA3.1-EGFP, while *FBXW7*, *SMURF2*, *TRIM25*, *WWP1*, *WWP2*, *HECW2*, *SMURF1*, and *NEDD4* were cloned into pcDNA3.1-mCherry, with *WWP2* also cloned into pcDNA3.1-Flag.

Cells were plated at a density of 5 × 10^5 cells per well in 6-well plates and cultured for 24 h prior to transfection. Transfection with the plasmids was performed using Lipofectamine 3000 (Invitrogen, USA).

2.15. Transmission electron microscopy (TEM)

Cells treated with or without BrA were fixed with 2.5% glutaraldehyde, post-fixed in 1% osmium tetroxide, dehydrated in graded ethanol, and embedded in epoxy resin. Ultrathin sections were stained with uranyl acetate and lead citrate, followed by observation under a transmission electron microscope. ER-mitochondria contact distance and association were quantified using ImageJ software.

2.16. Microscale thermophoresis (MST) assays

2.16.1. Direct binding assay

To evaluate the direct binding of BrA to KLF5 and candidate target proteins, including CCT3, PDIA3, RTCB, PHGDH, HMGCS1, SHMT2, and DNAJC7, MCF7 cells were transfected with the corresponding EGFP-tagged expression constructs for 48 h. Cell lysates containing EGFP-fusion proteins were collected and diluted in MST binding buffer (50 mmol·L^{-1} Tris-HCl, pH 7.4, 150 mmol·L^{-1} NaCl, 10 mmol·L^{-1} $MgCl_2$, and 0.05% Tween-20). The concentration of each EGFP-fusion protein was maintained at approximately 50 nmol·L^{-1}, while BrA was serially diluted in 16 steps from 0.015 to 500 μmol·L^{-1}. Protein-compound mixtures were then loaded into standard treated Monolith NT.115 capillaries for MST analysis [38]. The binding affinity (Kd) was measured using a Monolith NT.115 instrument (NanoTemper Technologies, Germany). Data were analyzed using MO. Affinity Analysis software (v2.3).

2.16.2. Evaluation of KLF5/E3 ligase interactions

To investigate the effect of BrA on KLF5-E3 ligase recruitment, purified recombinant KLF5 protein was pre-incubated with either 12.8 μmol·L^{-1} BrA or DMSO for 1 h at room temperature. Subsequently, these mixtures were incubated with lysates from MCF7 cells overexpressing various mCherry-tagged E3 ligases (FBXW7, SMURF2, TRIM25, WWP1, WWP2, HECW2, SMURF1, or NEDD4). After an additional 1 h incubation, the thermophoresis signal of the mCherry-labeled proteins was monitored. The shift in the binding curve or FNorm values was used to quantify the BrA-induced changes in the interaction between KLF5 and the respective E3 ligases. All experiments were performed in triplicate to ensure reproducibility [39].

2.17. RNA interference

Small interfering RNAs (siRNAs) specifically targeting KLF5 and WWP2 were designed and synthesized by GenePharma (Shanghai, China). The antisense sequences for KLF5 siRNAs were: siRNA#1, 5'-CAGAGATGCTCCAGAATTTTT-3' and siRNA#2, 5'-GCACAAAAGTTTATACCAATT-3'. For WWP2, the targeting sequences included: siRNA#1, 5'-GGTGCTCAACCCTATGTATTT-3'; siRNA#2, 5'-AGGAGGTTCTGCCTGTAATTT-3'; and siRNA#3, 5'-ACGGACGTGTCTATTATGTTT-3'. Cells were transfected with the indicated siRNAs using Lipofectamine 2000 (Invitrogen) following the manufacturer's instructions.

2.18. Real-time quantitative PCR (qPCR)

qPCR for *KLF5* mRNA expression, total RNA was extracted from cells and reverse transcribed into cDNA. qPCR was performed using SYBR® Green Master Mix (Vazyme, Shanghai, China) on a CFX96 platform (Bio-Rad, USA) according to the manufacturer's instructions. Relative *KLF5* mRNA expression was calculated using the $2^{-\Delta\Delta Ct}$ method, with *α-tubulin* as the reference gene [40].

2.19. Ubiquitination assay

To assess the ubiquitination level of KLF5, cells were first transfected with the indicated plasmids and/or siRNAs, followed by treatment with BrA. To stabilize ubiquitinated proteins, the cells were then exposed to the proteasome inhibitors PS-341 (100 nmol·L^{-1}) or MG-132 (1 μmol·L^{-1}) for indicated time, and subsequently to the deubiquitinase inhibitor PR-619 (20 μmol·L^{-1}) for 1 h. Cells were lysed under denaturing conditions, and the proteins of interest were immunoprecipitated using an anti-Myc antibody, as described previously [41].

2.20. Immunoprecipitation

Following transfection with the indicated constructs, cells were lysed using a commercial lysis buffer (Beyotime, China). The resulting lysates were subjected to immunoprecipitation with the specified antibodies, and the immunoprecipitated proteins were subsequently analyzed by Western blot [42].

2.21. Molecular docking and dynamics simulations

Molecular docking of BrA with an AlphaFold2-predicted KLF5 structure (prepared in UCSF Chimera, protonated at pH 7.4 *via* H^+) was performed using AutoDock 4.2. Molecular dynamics simulations (GROMACS 5.1.5) were then conducted to assess complex stability. The system (AMBER ff14SB, TIP3P water, 298.15 K, 1 bar) underwent energy minimization, NVT/NPT equilibration, and a 100 ns production phase. Resulting trajectories were analyzed for the root-mean-square deviation (RMSD), radius of gyration (Rg), solvent-accessible surface area (SASA), and root-mean-square fluctuation (RMSF) to evaluate binding stability.

2.22. Xenograft experiments

In vivo antitumor efficacy of BrA was evaluated using

zebrafish and mouse xenograft models, under a protocol approved by the Animal Ethics Committee of Hubei University of Medicine (2024-013; Feb 20, 2024).

In the zebrafish model, BrA was administered intravenously to embryos bearing CM-Dil-labeled MDA-MB-231 cell xenografts (200 cells/fish), with DDP (2.0 ng per fish) as a positive control.

In the mouse model, female nude mice (5-week-old, n = 32) were subcutaneously injected with MDA-MB-231 cells (5×10^6) and randomly assigned to four treatment groups receiving intraperitoneal injections every two days for four weeks: vehicle, BrA (3 mg·kg^{-1}), BrA (6 mg·kg^{-1}), or DDP (5 mg·kg^{-1}). Tumor growth was monitored by biweekly volume measurements. Serum biochemical parameters were measured to evaluate systemic toxicity. Cardiac injury was assessed by creatine kinase-MB (CK-MB) and lactate dehydrogenase (LDH); liver function by alanine aminotransferase (ALT), aspartate aminotransferase (AST), total protein (TP), and albumin (ALB); and renal function by creatinine (CRE) and blood urea nitrogen (BUN). Tumors and key organs (heart, liver, spleen, lung, kidney) were excised for histological (H&E), immunohistochemical (IHC) analyses.

2.23. Toxicological evaluation of BrA in zebrafish

BrA was evaluated for hepatotoxicity and cardiotoxicity in zebrafish. Tg(fabp10 : EGFP) larvae (3 dpf) were injected with BrA and incubated for 48 h; liver size and fluorescence were then imaged and quantified. For cardiotoxicity, AB strain larvae (2 dpf) were treated with BrA for 4 h, followed by assessment of heart rate, circulation, hemorrhage, and thrombosis. Dose-mortality relationships for both assays were analyzed with Origin 8.0, and toxic events were statistically evaluated.

2.24. Statistical analysis

All the statistical analyses were conducted using GraphPad Prism 9. Statistically significant values were compared using Student's t test. $P < 0.05$ indicated a statistically significant difference.

3. Results

3.1. BrA inhibits growth in BC

We first assessed the cytotoxic effect of BrA on BC cells and non-tumorigenic MCF-10A cells. CCK-8 assays demonstrated that BC cells were more sensitive to BrA than MCF-10A cells, based on IC_{50} values, with DDP serving as a positive control (Fig. 1A). Moreover, RTCA confirmed that BrA reduced the number of viable BC cells (Fig. 1B). Notably, BrA also markedly suppressed the clonogenic ability of BC cells (Figs. 1C, 1D). High-content analysis further revealed that BrA induced significant morphological alterations, including a concentration-dependent reduction in cell area and a corresponding increase in cell roundness (Figs. 1E–1G). These findings collectively indicate that BrA possesses a potent growth-suppressive activity in BC.

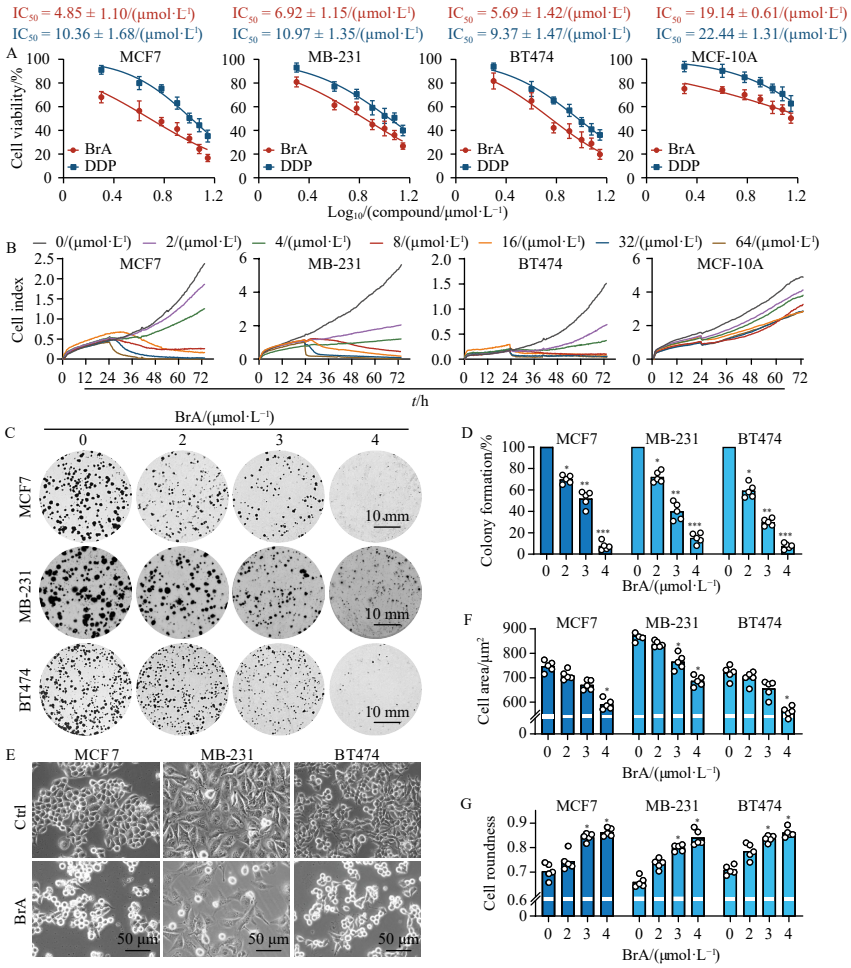


Fig. 1 BrA inhibits growth in BC cells. (A) Viability of BC cells and non-tumorigenic MCF-10A cells treated with BrA, measured by CCK-8 assay. (B) RTCA of BrA's inhibitory effect on BC cell proliferation. (C, D) Clonogenic survival of BC cells following BrA treatment. Scale bar,10 mm. (E-G) High-content analysis of BC cells. Quantitative analysis of cell area (F) and roundness (G) is shown. Scale bar, 50 μm. Data were expressed as mean ± SD (n = 5). $^{*}P < 0.05$, $^{**}P < 0.01$, $^{***}P < 0.001$ *vs* 0 μmol·L^{-1}.

3.2. BrA induces mitochondrial dysfunction in BC cells

To elucidate the mechanism by which BrA acts on BC, RNA-seq was performed in BT474 cells treated with BrA. Transcriptomic profiling revealed that BrA significantly upregulated 652 genes and downregulated 765 genes (Fig. 2A). KEGG pathway analysis identified oxidative phosphorylation, the citrate cycle (TCA), and protein processing in the ER as the major pathways significantly affected by BrA treatment (Fig. 2B). Gene set enrichment analysis (GSEA) further demonstrated that both oxidative phosphorylation and the TCA were negatively enriched (Fig. 2C), suggesting that BrA may suppress energy metabolism in BC cells.

To further investigate the impact of BrA on mitochondrial function, we assessed mitochondrial permeability using calcein-AM staining. BrA treatment markedly reduced mitochondrial calcein-AM fluorescence, indicating enhanced opening of the mPTP (Fig. 2D). Consistently, BrA significantly elevated mitoROS levels, as evidenced by increased MitoSOX Red fluorescence (Fig. 2E). Given that excessive mPTP opening is often associated with mitochondrial damage, mitochondrial morphology was examined using Mito-DsRed. BrA induced pronounced mitochondrial fragmentation, characterized by an abundance of short, rod-like, and punctate mitochondria (Figs. 2F, 2G), indicative of increased mitochondrial fission.

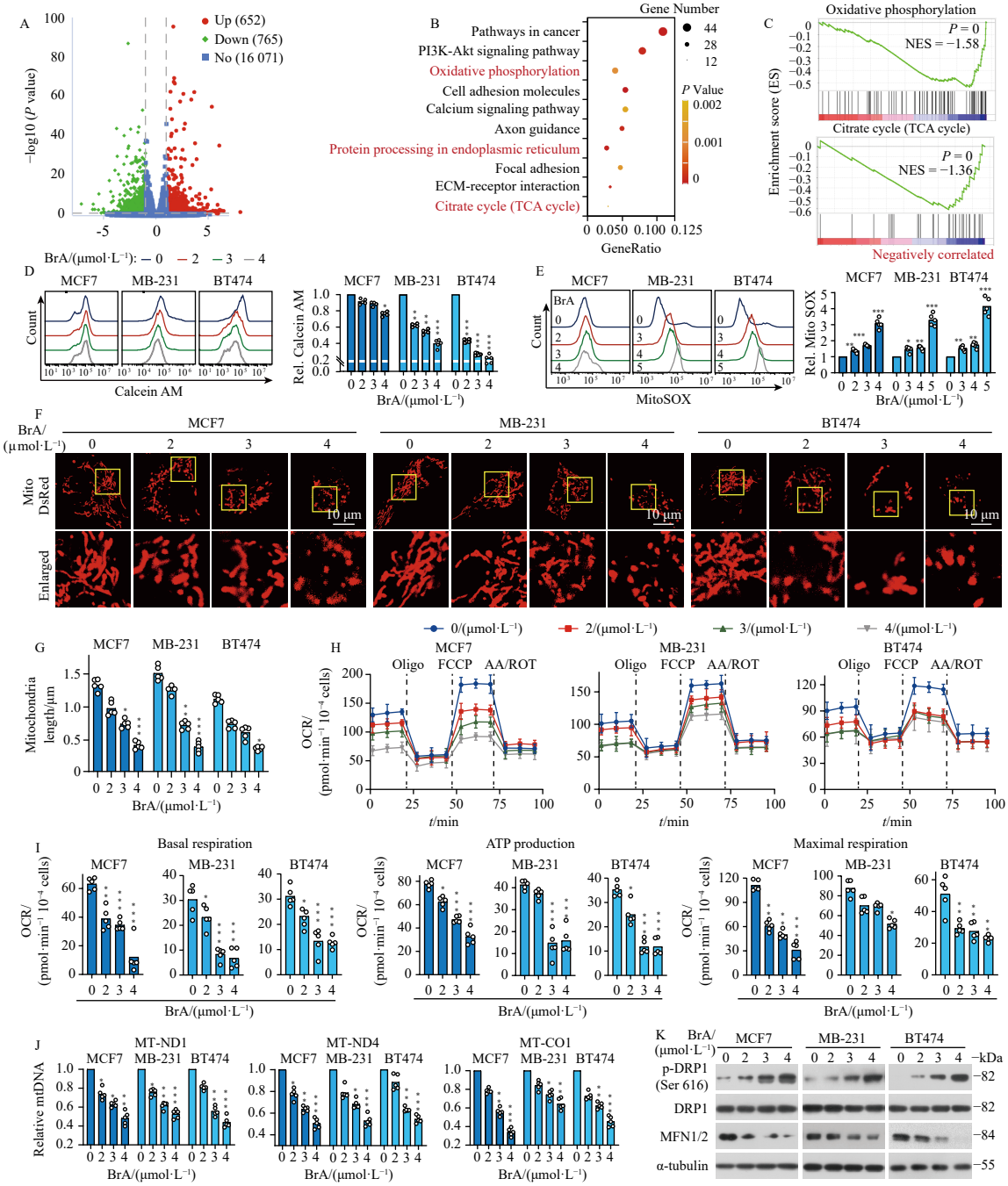


Fig. 2 BrA induces mitochondrial dysfunction in BC cells. (A-C) Transcriptomic profiling of BT474 cells treated with or without BrA using RNA sequencing. (A) Volcano plot of differentially expressed genes; (B) KEGG pathway enrichment analysis; (C) GSEA pathway enrichment analysis. (D-G) Cells were treated with BrA for 24 h. (D) mPTP opening was measured by flow cytometry using calcein AM dye. (E) mitoROS accumulation was analyzed by flow cytometry after MitoSOX Red staining. (F) Mitochondrial morphology was visualized by confocal microscopy in Mito-DsRed-expressing cells. Scale bar, 10 μm. (G) Average mitochondrial length was quantified (5 cells per experiment). (H, I) OCR was measured using a Seahorse XFe24 analyzer, and basal respiration, ATP production, and maximal respiration were quantified. (J) mtDNA expression was determined by qPCR. (K) Mitochondrial fusion/fission proteins were detected by Western blot. Data were expressed as mean ± SD (n = 5). $^{*}P < 0.05$, $^{**}P < 0.01$, $^{***}P < 0.001$ *vs* 0 μmol·L^{-1}.

Seahorse analysis further revealed that BrA markedly suppressed the OCR, reflecting impaired mitochondrial respiration (Figs. 2H, 2I). In line with this, quantitative PCR analysis showed a substantial reduction in mtDNA copy number following BrA treatment (Fig. 2J). Western blot analysis demonstrated that BrA downregulated mitochondrial fusion proteins MFN1/2 and increased DRP1 phosphorylation, a hallmark of mitochondrial fission (Fig. 2K). Collectively, these findings indicate that BrA disrupts mitochondrial dynamics and compromises mitochondrial function in BC cells.

3.3. BrA promotes ER-mitochondria contact-associated ER stress in BC cells

In line with the KEGG findings, our GSEA results also showed that BrA treatment induced significant enrichment in gene sets related to the cellular response to unfolded proteins and the intrinsic apoptotic signaling pathway in response to ER (Fig. 3A). Heatmap analysis also demonstrated the top 20 most significantly upregulated genes associated with ER stress (Fig. 3B). To determine whether BrA induces ER stress in BC cells, ER-Tracker staining was first performed, revealing increased ER signal intensity upon BrA treatment (Fig. 3C). Consistently, Western blot analysis demonstrated significant upregulation of the ER chaperone Bip and transcription factor ATF4, along with enhanced phosphorylation of PERK and EIF2α (Fig. 3D), key mediators of the unfolded protein response. These findings indicate that BrA activates ER stress signaling pathways.

Considering that mitoROS causes ER stress, we speculate that BrA not only disrupts mitochondrial function but may also promote ER stress through mitoROS. To explore the role of mitoROS in BrA-induced ER stress, BC cells were co-treated with BrA and the mitochondrial-targeted antioxidant Mito-TEMPO. MitoSOX staining confirmed that Mito-TEMPO effectively suppressed BrA-induced mitoROS production (Fig. 3E). Correspondingly, ER-Tracker staining showed attenuation of ER stress signals following Mito-TEMPO co-treatment (Fig. 3F). Western blot analysis further revealed that Mito-TEMPO reversed the BrA-induced upregulation of ATF4, as well as the phosphorylation of PERK and EIF2α (Fig. 3G). Functionally, CCK-8 assays demonstrated that

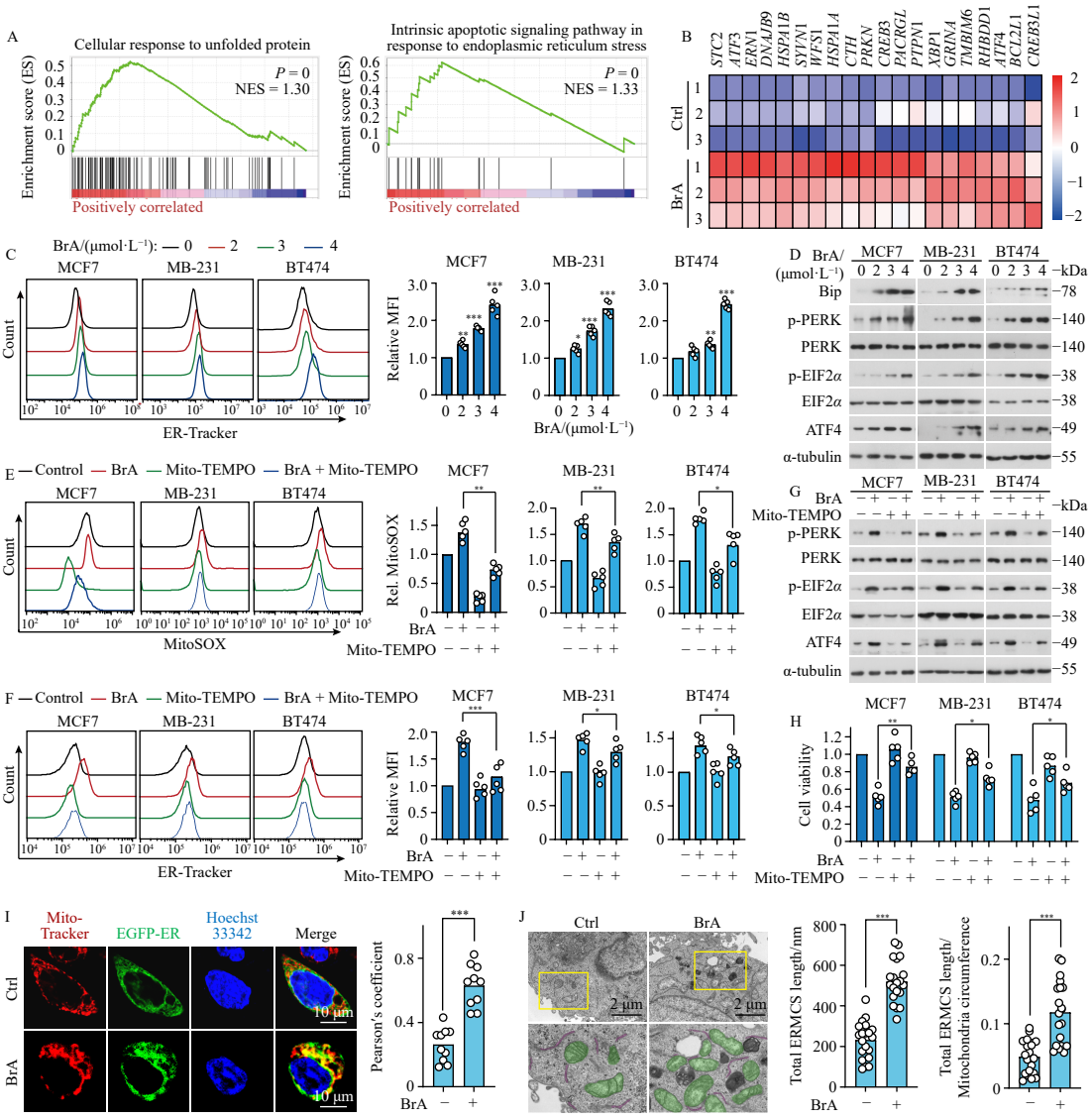


Fig. 3 BrA promotes ER-mitochondria contact-associated ER stress in BC cells. (A) GSEA of RNA-Seq. (B) Heatmap of the top 20 upregulated genes in the cellular response to unfolded protein and intrinsic apoptotic signaling pathways. (C-G) Cells were treated with BrA for 24 h. (C) ER signal intensity was analyzed by flow cytometry after ER-Tracker staining. (D) ER stress markers were detected by Western blot. (E-H) Cells were cotreated with BrA (3 μmol·L^{-1}) and Mito-TEMPO (5 μmol·L^{-1}) for 24 h, then mitoROS (E) and ER stress (F) was analyzed by flow cytometry, protein expression was detected by Western blot (G), cell growth was detected by CCK-8 assay (H). (I, J) MCF7 cells were treated with BrA for 24 h. (I) ER-mitochondria colocalization was assessed by confocal microscopy in EGFP-ER-transfected cells stained with Mito-Tracker. Scale bar, 10 μm. (J) ERMCS length and its ratio to mitochondrial circumference were assessed by TEM. Scale bar, 2 μm. Data were expressed as mean ± SD (n = 5). $^{*}P < 0.05$, $^{**}P < 0.01$, $^{***}P < 0.001$ *vs* BrA group.

scavenging mitoROS partially rescued BrA-induced inhibition of BC cell proliferation (Fig. 3H). These results suggest that mitoROS act as upstream mediators of ER stress and growth inhibition in BrA-treated BC cells.

To investigate the effect of BrA on ER-mitochondria interactions, live-cell imaging was performed using EGFP-ER and Mito-Tracker staining. Colocalization analysis showed that BrA markedly enhanced ER-mitochondria coupling in BC cells (Fig. 3I). Consistently, TEM analysis revealed increased ER-mitochondria contact site (ERMCS) length and the total ERMCS length relative to mitochondrial circumference after BrA treatment (Fig. 3J). These findings suggest that BrA promotes ER-mitochondria contact, which may contribute to mitoROS accumulation and ER stress activation in BC cells.

3.4. BrA induces mitochondrial dysfunction and ER stress by downregulating KLF5

To elucidate the molecular target underlying the anti-BC activity of BrA, DARTS assays were conducted (Fig. 4A). Co-incubation of BrA with BC cell lysates resulted in increased stability of several protein bands (Fig. 4B). Mass spectrometry analysis of these protected bands identified KLF5 as a high-confidence binding candidate (Fig. 4C). MST further verified a direct and specific interaction between BrA and KLF5, with a Kd of 0.66 μmol·L^{-1} (Fig. 4D). Molecular docking analysis revealed that BrA binds to KLF5 through two hydrogen bonds formed with residues P131 and Y112, with bond distances of 3.5 Å and 3.1 Å, respectively (Fig. 4E). Western blot analysis showed that BrA markedly reduced KLF5 protein levels in BC cells (Fig. 4F). To determine whether KLF5 mediates the inhibitory effects of BrA, KLF5 was overexpressed in BC cells (Fig. 4G). Calcein-AM staining demonstrated that KLF5 overexpression attenuated BrA-induced opening of the mPTP (Fig. 4H). Seahorse OCR analysis further revealed that KLF5 restored mitochondrial respiration suppressed by BrA (Figs. 4I, 4J). Similarly, ER-Tracker staining indicated that KLF5 overexpression alleviated BrA-induced ER stress (Fig. 4K). At the molecular level, Western blot analysis confirmed that KLF5 overexpression reversed BrA-mediated alterations in mitochondrial dynamics, including decreased DRP1 phosphorylation and restoration of MFN1/2 expression (Fig. 4L). Moreover, KLF5 effectively inhibited BrA-induced activation of the PERK-EIF2α branch of the unfolded protein response, as evidenced by reduced phosphorylation of these ER stress markers (Fig. 4M). Functional validation using RTCA demonstrated that KLF5 overexpression significantly protected BC cells from BrA-induced loss of viability (Fig. 4N). Conversely, KLF5 silencing largely neutralized the modulatory effects of BrA on mitochondrial function, ER homeostasis, and cell proliferation (Fig. S1), further confirming that KLF5 is a requisite mediator of BrA-induced cytotoxicity. Together, these data suggest that BrA disrupts mitochondrial function and ER homeostasis in BC cells in a KLF5-dependent manner.

3.5. BrA reduces KLF5 protein stability through WWP2-mediated ubiquitination

Then, qPCR was performed to confirm the BrA-induced downregulation of KLF5 protein expression. The data indicated that BrA has no significant effect on *KLF5* mRNA expression (Fig. 5A). We assumed that BrA may influence KLF5 protein stability. Proteasome inhibitors (MG-132 and PS-341) were used to block protein degradation in BC. The results indicated that MG-132 or PS-341 significantly antagonized the BrA-induced degradation of KLF5 (Fig. 5B). A ubiquitination assay suggested that BrA increased the level of ubiquitinated KLF5 (Fig. 5C). These results suggested that BrA induces KLF5 degradation *via* the ubiquitin-proteasome pathway. Next, we further hypothesized that BrA may promote KLF5 degradation by affecting E3 ubiquitin ligase. Based on the UbiBrowser database, which provides comprehensive information on E3 ubiquitin ligase-substrate interactions, we identified four known E3 ligases (FBXW7, SMURF2, TRIM25, and WWP1) that mediate KLF5 degradation. Additionally, we included the top four E3 ligases (WWP2, HECW2, SMURF1, and NEDD4) predicted by UbiBrowser (Fig. 5D). Using MST assays, we examined the effect of BrA on the binding of these E3 ligases to KLF5. The results showed that BrA significantly enhanced the binding of WWP2 to KLF5, with the Kd decreasing from 4.99 μmol·L^{-1} to 0.07 μmol·L^{-1} (Fig. 5E). Co-IP analysis further confirmed that BrA facilitated the interaction between WWP2 and KLF5 (Fig. 5F). Moreover, ubiquitination assays demonstrated that WWP2 knockdown effectively inhibited the BrA-induced increase in KLF5 ubiquitination (Fig. 5G). To identify the interacting domains, we performed truncation mutagenesis and co-IP assays. These experiments mapped the WWP2-binding region on KLF5 to its central domain (202–372 aa) and further revealed that the WW domain of WWP2 is essential for its interaction with KLF5 (Figs. 5H–5K). Ubiquitin possesses seven lysine residues, with K48-linked chains primarily driving proteasomal degradation [43]. To identify the KLF5 ubiquitination linkage type, we co-transfected BC cells with HA-KLF5, Flag-WWP2, and Myc-Ub constructs (Ub^{K11}, Ub^{K48}, or Ub^{K63}). KLF5 ubiquitination was markedly enhanced specifically by Ub^{K48} (Fig. 5L), confirming that KLF5 undergoes K48-linked ubiquitination. Furthermore, within the WWP2-binding region of KLF5 (202–372 aa), we targeted potential lysine residues (K209, K276, K335, and K369) *via* site-directed mutagenesis. Ubiquitination assays using K-to-R mutants revealed that the K335R mutation significantly abolished WWP2-mediated K48-linked ubiquitination of KLF5 (Fig. 5M), suggesting that K335 is the primary acceptor site for WWP2-mediated K48-linked polyubiquitination of KLF5. Collectively, these findings suggest that BrA promotes WWP2-mediated ubiquitination and proteasomal degradation of KLF5 by enhancing the binding of WWP2 to KLF5.

Next, molecular dynamics simulations were performed to determine the effect of BrA on WWP2 and KLF5 binding (Fig. S2A-S2E). RMSD, Rg, and SASA analyses revealed that these parameters were significantly smaller for the protein in the KLF5-WWP2-BrA system than in the KLF5-WWP2 system (Fig. S2B-S2D), indicating that BrA stabilizes the binding between KLF5 and WWP2. In addition, RMSF analysis showed that BrA binding reduced the flexibility of key residues within KLF5 (Fig. S2E). This induced rigidity correlates with enhanced stability of the KLF5-WWP2 complex. Corroborating this observation, binding energy calculations demonstrated a more favorable free energy for the KLF5-WWP2-BrA system (−95.03 kcal·mol^{-1}) compared to the KLF5-WWP2 system (−58.53 kcal·mol^{-1}) (Table 2), indicating that BrA stabilizes the binding configuration between KLF5 and WWP2.

3.6. Inhibitory effect of BrA on xenograft tumors

To evaluate the anticancer efficacy of BrA *in vivo*, we established a zebrafish xenograft model. A preliminary dose-ranging study determined the maximum tolerated dose (MTD) of BrA in zebrafish to be 25 ng per fish. Based on this, three treatment doses were selected for the efficacy study: 6.25 ng per fish (MTD/4), 12.5 ng per fish (MTD/2), and 25 ng per fish (MTD). DDP (2.0 ng per fish) was included as a positive control. The results demonstrated that BrA treatment led to a significant and dose-dependent reduction in tumor size compared to the control group (Figs. 6A, 6B).

The antitumor activity of BrA was further evaluated in a murine subcutaneous xenograft model using MDA-MB-231 cells. Tumor growth was markedly suppressed in both the low-dose (BrA-L, 3 mg·kg^{-1}) and high-dose (BrA-H, 6 mg·kg^{-1}) groups, compar-

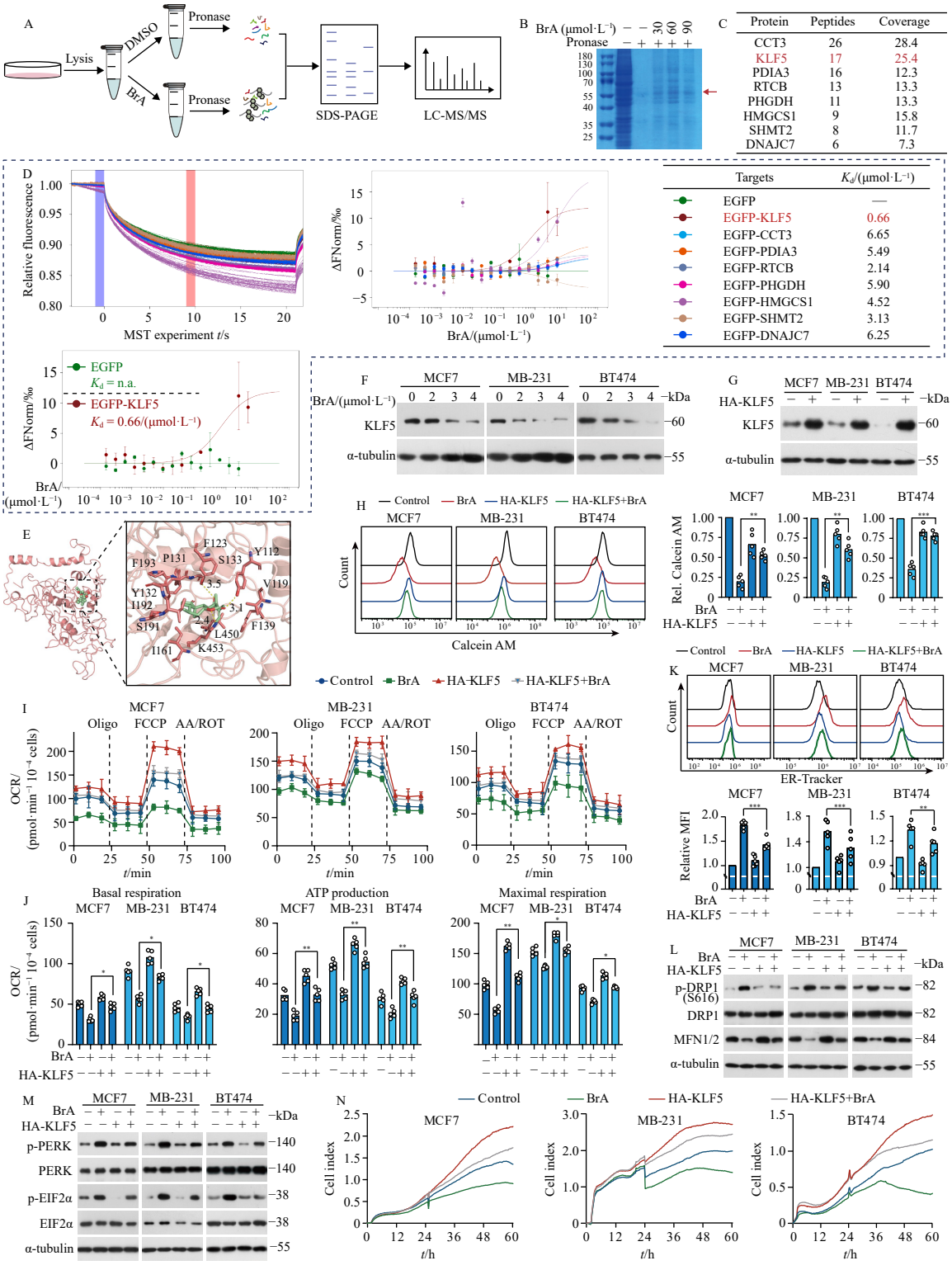
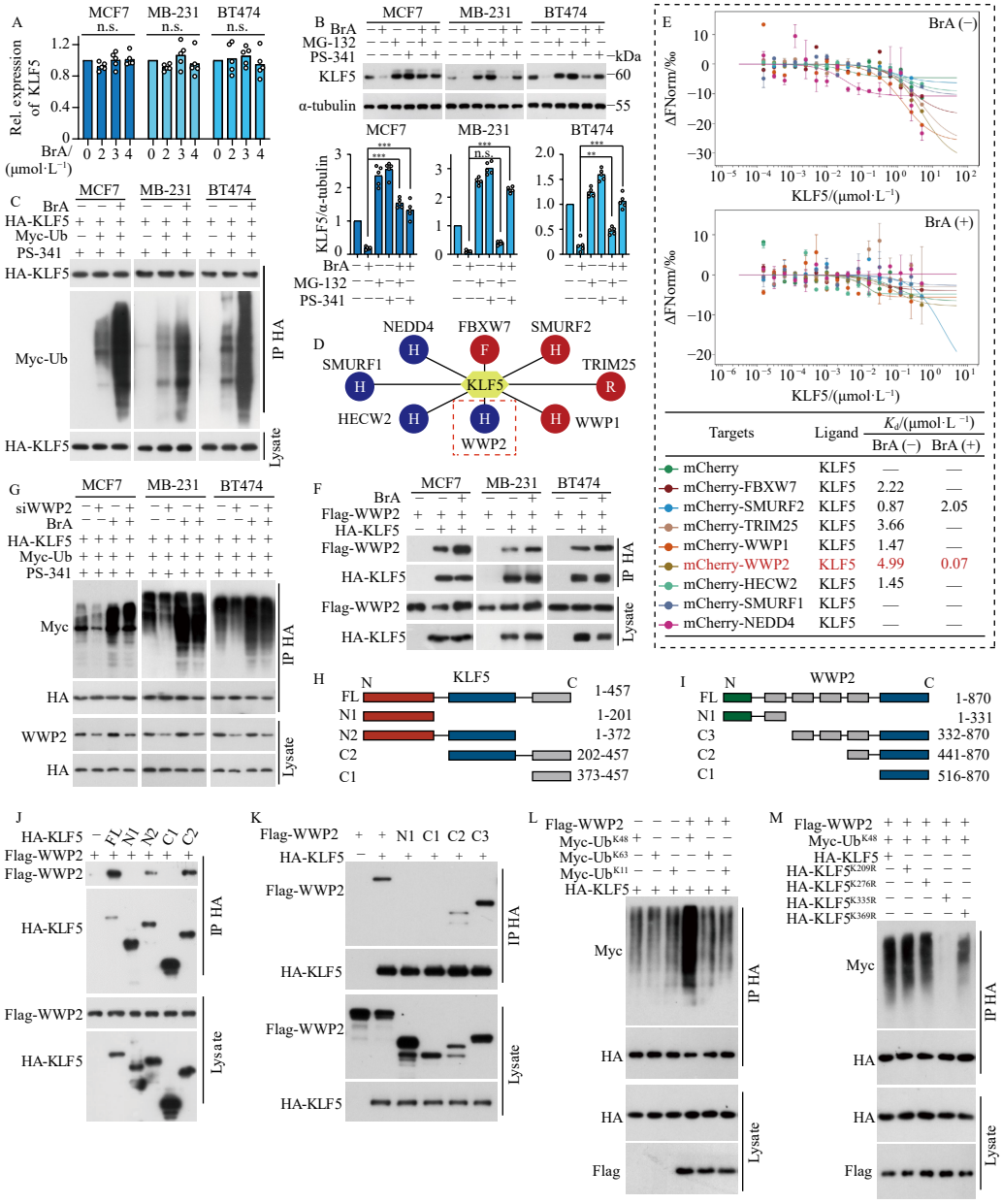


Fig. 4 BrA induces mitochondrial dysfunction and ER stress by downregulating KLF5. (A) Schematic diagram of DARTS-MS technology. (B, C) DARTS-MS identification of the cellular target of BrA in BT474 cells. (D) MST analysis of the binding affinity between BrA and candidate targets identified by DARTS-MS. (E) Binding pose of BrA with KLF5 from molecular docking simulation, highlighting the key interacting residues. (F) Cells were treated with BrA for 24 h. Then, Western blot was performed. (G) Validation of HA-KLF5 overexpression by Western blot analysis. (H) Cells were transfected with HA-KLF5 for 24 h and then treated with BrA (5 μmol·L^{-1}) for 24 h. mPTP opening was measured with flow cytometry using Calcein AM dye. (I–N) Cells were transfected with HA-KLF5 for 24 h and then treated with BrA (3 μmol·L^{-1}) for 24 h. The OCR was detected with a Seahorse XFe24 (I, J), ER stress was measured with flow cytometry using ER-Tracker (K), protein expression was detected by Western blot (L, M), and cell viability was evaluated using RTCA (N). Data were expressed as mean ± SD (n = 5). $^{*}P$ < 0.05, $^{**}P$ < 0.01, $^{***}P$ < 0.001. BrA group *vs* HA-KLF5 + BrA group.

able to the effect observed in the DDP-treated group (5 mg·kg^{-1}) (Figs. 6C–6F). IHC analysis of tumor tissues showed a significant reduction in KLF5 and Ki67 expression in BrA-treated mice, consistent with its mechanism of action observed *in vitro* (Fig. 6G). In terms of safety, BrA treatment had no adverse effect on body weight throughout the study (Fig. 6H). Furthermore, serum biochemical indices (including CK-MB, LDH, ALT, AST, TP, ALB, CRE, and BUN) remained within normal ranges across all treatment groups, indicating that BrA did not cause heart, liver, spleen, or renal toxicity (Fig. 6I). Histopathological evaluation using H&E staining revealed no significant tissue damage in the heart, liver, spleen, lung, or kidneys (Fig. 6J). Collectively, these findings in-



Targets	Ligand	K_d/(μmol·L⁻¹) BrA (−)	K_d/(μmol·L⁻¹) BrA (+)
mCherry	KLF5	—	—
mCherry-FBXW7	KLF5	2.22	—
mCherry-SMURF2	KLF5	0.87	2.05
mCherry-TRIM25	KLF5	3.66	—
mCherry-WWP1	KLF5	1.47	—
mCherry-WWP2	KLF5	4.99	0.07
mCherry-HECW2	KLF5	1.45	—
mCherry-SMURF1	KLF5	—	—
mCherry-NEDD4	KLF5	—	—

Fig. 5 BrA reduces KLF5 protein stability through WWP2-mediated ubiquitination. (A) Cells were treated with BrA for 24 h. qPCR was then performed. (B) Cells were treated with PS-341 (100 nmol·L^{-1})/MG-132 (1 μmol·L^{-1}) for 6 h and then treated with BrA (3 μmol·L^{-1}) for 24 h. Western blot was performed. (C) Cells were transfected with HA-KLF5 and Myc-Ub for 6 h, treated with BrA (3 μmol·L^{-1}) for 24 h and lysed. The lysates were immunoprecipitated as indicated. (D) UbiBrowser web services analyze ubiquitin ligases that mediate KLF5 protein degradation. (E) MST assays were performed to evaluate the interaction between recombinant KLF5 protein and mCherry-tagged E3 ligases in the presence or absence of BrA. (F) Co-IP analysis of the interaction between HA-KLF5 and Flag-WWP2 following BrA treatment. (G) Cells were transfected with WWP2 siRNA (siWWP2) for 24 h, followed by co-transfection with HA-KLF5 and Myc-Ub, and BrA treatment for an additional 24 h. Immunoprecipitation was then performed to assess KLF5 ubiquitination. (H, I) Schematic representation of KLF5, WWP2, and their mutant constructs. (J, K) HEK293T cells were cotransfected with the indicated constructs for 48 h. Co-IP was performed using HA beads, followed by Western blot. (L) MCF7 cells co-transfected with HA-KLF5, Myc-tagged ubiquitin mutants (K11, K48, or K63), and Flag-empty vector or Flag-WWP2 were treated with PS-341 for 24 h. HA-immunoprecipitated lysates were immunoblotted with anti-Myc to detect ubiquitinated KLF5. (M) MCF7 cells were co-transfected with Flag-WWP2, Myc-Ub^{K48} ubiquitin, and HA-KLF5 (wild-type or K209R/K276R/K335R/K369R mutants), treated with PS-341 for 24 h, and then subjected to HA-IP and Myc-immunoblotting. Data were expressed as mean ± SD (n = 5). n.s., not significant. $^{**}P < 0.01$, $^{***}P < 0.001$ BrA group *vs* MG-132 + BrA group/PS-341 + BrA group.

Table 2 MM/GBSA binding free energy (kcal·mol^{-1}) of simulation systems.

System	ΔE_{vdw}	ΔE_{ele}	ΔE_{GB}	ΔE_{SURF}	ΔG_{GAS}	ΔG_{solv}	ΔG_{bind}
KLF5-BrA	−37.69 ± 2.54	−6.34 ± 1.31	8.51 ± 0.86	−5.01 ± 0.18	−44.02 ± 2.15	3.50 ± 0.79	−40.53 ± 2.05
KLF5-WWP2	−123.77 ± 16.42	−104.16 ± 13.30	168.72 ± 24.22	−9.74 ± 0.71	−227.51 ± 11.19	158.98 ± 15.21	−58.53 ± 6.15
KLF5-WWP2-BrA	−131.14 ± 15.72	−106.02 ± 14.00	152.00 ± 21.60	−9.87 ± 0.60	−237.16 ± 16.63	142.13 ± 14.63	−95.03 ± 8.73

dicate that BrA exhibits favorable *in vivo* tolerability and minimal systemic toxicity.

3.7. Toxicological evaluation of BrA in zebrafish

To evaluate the toxicity of BrA to the heart and liver, we used a zebrafish toxicity assay. In the liver toxicity evaluation, after intravenous injection of increasing doses of BrA, the maximum nonlethal dose (MNLD) and 10% lethal dose (LD_{10}) of BrA in zebrafish were 82.1 and 86.0 ng per fish, respectively. Subsequently, BrA doses of 9.12 ng per fish (1/9 MNLD), 27.4 ng per fish (1/3 MNLD), and 82.1 ng per fish (MNLD) were selected for

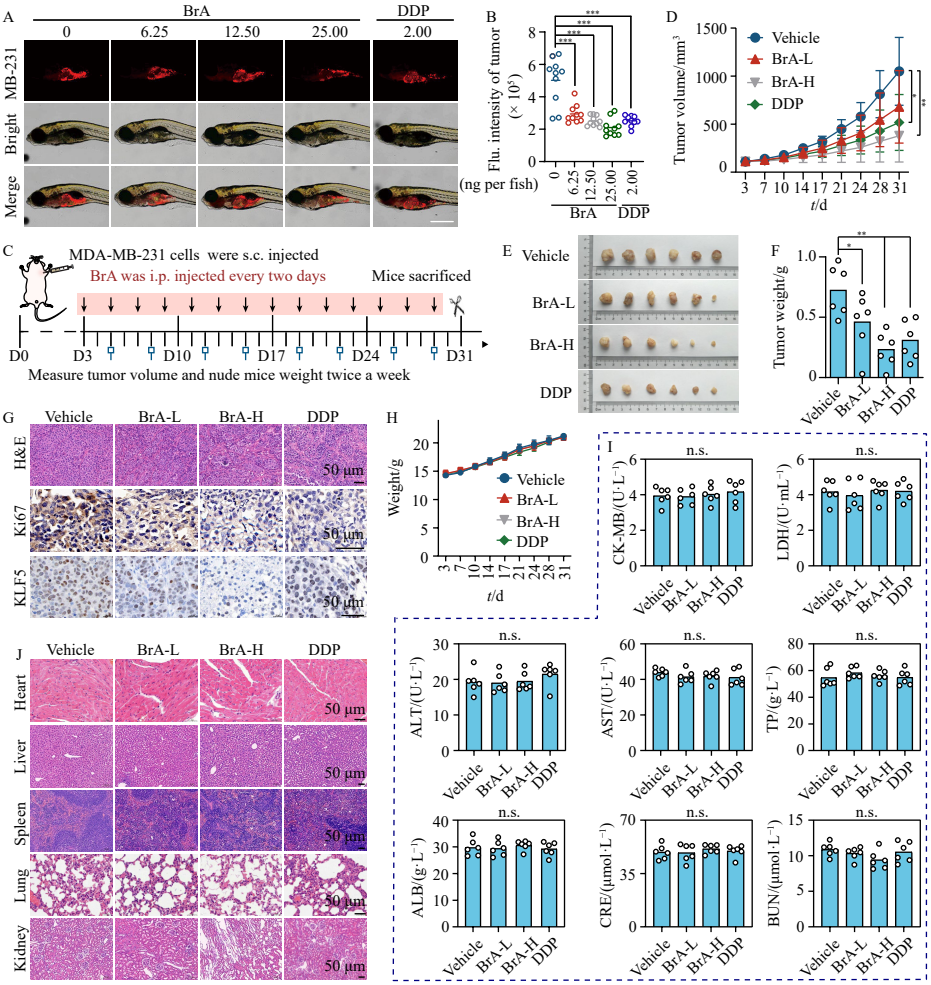


Fig. 6 Inhibitory effect of BrA on xenograft tumors. (A, B) MDA-MB-231 cell-derived xenografts in zebrafish larvae were treated with BrA or DDP at the indicated concentrations and imaged at 2 dpi. Red fluorescence intensity reflects tumor burden. Scale bar, 400 μm. (C, D) Tumor volumes in MDA-MB-231 cell-derived xenograft nude mice following treatment with low-dose BrA (BrA-L, 3 mg·kg^{-1}), high-dose BrA (BrA-H, 6 mg·kg^{-1}), or DDP (5 mg·kg^{-1}). (E) Representative images of excised xenograft tumors from each treatment group. (F) Tumor weights of the sacrificed mice. (G) Tumor sections were analyzed by H&E staining and IHC. Scale bar, 50 μm. (H) Body weights of mice during treatment were recorded to assess systemic toxicity. (I) Serum biochemical parameters were measured to evaluate systemic toxicity. (J) Histological examination of heart, liver, spleen, lung, and kidney tissues using H&E staining. Scale bar, 50 μm. Data were expressed as mean ± SD ($n \geq 6$). n.s., not significant. $^{*}P < 0.05$, $^{**}P < 0.01$, $^{***}P < 0.001$ Vehicle group *vs* BrA group/DDP group.

the formal tests. The results showed that BrA at 82.1 ng per fish induced hepatotoxicity (Figs. 7A–7D). In the cardiovascular toxicity evaluation, after intravenous injection of increasing doses of BrA, the MNLD and LD_{10} were determined to be 82.7 and 86.4 ng per fish, respectively (Fig. 7E). Subsequently, BrA doses of 9.19 ng per fish (1/9 MNLD), 27.6 ng per fish (1/3 MNLD), and 82.7 ng per fish (MNLD) were selected for the formal tests. The results showed that BrA induced cardiovascular toxicity, mainly manifested as pericardial edema, abnormal heart rhythm (reduced heart rate), slow blood flow, loss of circulation, and hemorrhage, with the lowest inducing dose being 82.7 ng per fish (Table 3, Figs. 7F, 7G). Overall, BrA overdose may cause hepatotoxicity and cardiac injury.

4. Discussion

In this study, we investigated the tumor-suppressive role of the natural sesquiterpene BrA in BC. Our findings demonstrate that (a) BrA markedly suppresses BC growth both *in vivo* and *in vitro*; (b) BrA induces mitochondrial dysfunction and ER stress in BC cells; (c) BrA directly targets and binds to KLF5; (d) BrA inhibits mitochondrial dysfunction and ER stress by targeting KLF5, thereby restraining BC growth; and (e) BrA promotes the direct interaction between KLF5 and the E3 ubiquitin ligase WWP2, leading to proteasomal degradation of KLF5 (Fig. 8). Collectively, these results uncover a previously unrecognized molecular mechanism by which BrA exerts its antitumor activity through KLF5 targeting in BC.

Mitochondrial dysfunction and ER stress play critical roles in the initiation and progression of BC [44]. As the central organelle for energy metabolism and apoptosis signaling, mitochondrial dysfunction often results in excessive ROS accumulation, which in turn activates cellular stress responses that affect tumor proliferation, migration, and therapy resistance [45]. Meanwhile, ER stress, primarily mediated through the UPR, can exert dual effects: transient activation promotes tumor adaptation, whereas sustained stress leads to apoptosis [46]. Our study further reinforces this concept, showing that BrA induces mitochondrial dysfunction and mitoROS production in BC cells, which in turn triggers ER stress and inhibits tumor cell growth. Notably, live-cell imaging and TEM analysis demonstrated that BrA enhanced ER-mitochondria contact, which may facilitate mitoROS accumulation and ER stress activation. These findings underscore the critical role of functional crosstalk between mitochondria and the ER in determining BC cell fate. Importantly, BrA emerges as a potential therapeutic agent capable of linking cellular stress signaling with energy metabolism by simultaneously disrupting mitochondrial function and ER homeostasis.

KLF5, a pivotal transcription factor regulating cell proliferation, differentiation, and tumorigenesis, is tightly controlled by

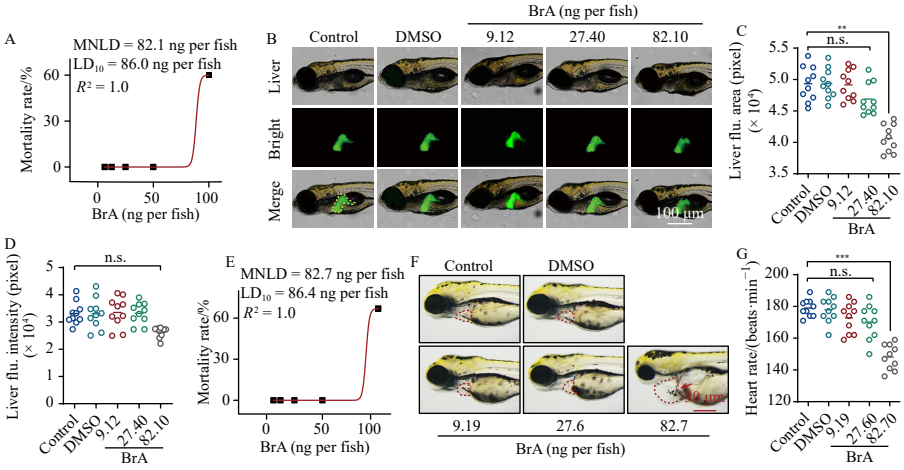


Fig. 7 Toxicological evaluation of BrA in zebrafish. (A) Liver toxicity "dose-mortality" curve of BrA in zebrafish. (B) Typical diagram of zebrafish liver toxicity after BrA treatment. (C, D) Liver fluorescence area and liver fluorescence analysis of the livers of BrA-treated zebrafish at 48 hpe. (E) Heart toxicity "dose-mortality" curve of BrA in zebrafish. (F) Typical diagram of zebrafish heart toxicity after BrA treatment. (G) Heart rate of zebrafish treated with BrA at 48 hpe. Data were expressed as mean ± SD (n = 10). n.s., not significant. $^{**}P < 0.01$, $^{***}P < 0.001$ *vs* control.

Table 3 Cardiovascular toxicity of BrA in zebrafish.

Type of malformation		Control	DMSO	BrA (ng per fish)		
				9.19	27.6	82.7
Heart	Pericardial edema	-	-	-	-	70% (21/30)
	Arrhythmia	-	-	-	-	70% (21/30)
Blood circulation	Slow-flow	-	-	-	-	70% (21/30)
	Blood circulation disorder	-	-	-	-	-
Bleeding		-	-	-	-	-
Thrombus		-	-	-	-	-

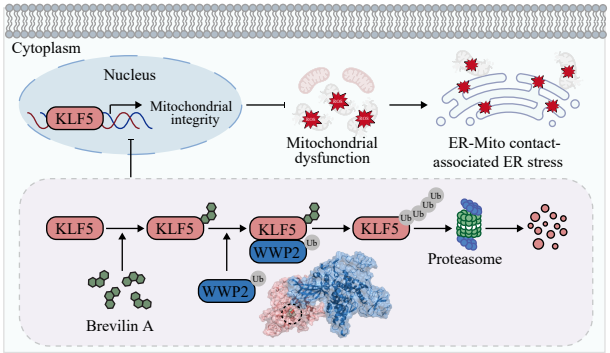


Fig. 8 Schematic illustration of the proposed mechanism of BrA action. BrA directly binds to KLF5 and promotes its interaction with WWP2, which facilitates KLF5 degradation *via* the proteasome. Degradation of KLF5 disrupts mitochondrial integrity, leading to mitochondrial dysfunction and subsequent ER stress.

the UPS [21]. Multiple E3 ligases, including WWP1, FBXW7, NEDD4L, and EFP, have been reported to target KLF5 for ubiquitination and degradation under distinct biological contexts. For example, WWP1 recognizes the PY motif of KLF5 through its WW domain, while TAZ can competitively block this interaction to stabilize KLF5 and promote its transcriptional activity [23]. In parallel, FBXW7 mediates GSK3β-dependent phosphorylation–ubiquitination of KLF5, as observed in metformin-treated TNBC cells, thereby suppressing cancer stemness [24]. NEDD4L promotes ferroptosis and radiosensitivity in esophageal squamous cell carcinoma by ubiquitinating and destabilizing KLF5 [47], whereas in ER-positive BC, estrogen induces EFP to facilitate KLF5 proteasomal degradation and modulate estrogen signaling [26]. These findings underscore that the stability of KLF5 is dynamically regulated by diverse upstream signals and ligases, with critical implications for tumor progression and therapeutic response. Our current study further expands this regulatory network, showing that BrA directly binds to KLF5 and specifically promotes the interaction between the PY motif and the WW domain, facilitating its association with WWP2 rather than other known E3 ubiquitin ligases, thereby driving KLF5 ubiquitination and proteasomal degradation. This mechanism differs from previously reported pathways, suggesting that natural compounds like BrA can selectively modulate KLF5 turnover by altering its conformation to favor unique E3 ligase interactions. Importantly, BrA-mediated KLF5 degradation disrupts its oncogenic transcriptional programs, inducing mitochondrial dysfunction and ER stress in BC cells, ultimately inhibiting tumor cell growth.

Notably, although hepatotoxicity and cardiovascular toxicity were observed in zebrafish at the MNLD dose level, no significant alterations in hepatic injury markers (ALT/AST) or the cardiac injury marker CK-MB were detected in BrA-treated mice, suggesting acceptable *in vivo* tolerability at the therapeutic dose used in this study. Nevertheless, further systematic safety evaluation is still warranted before clinical translation.

5. Conclusions

In summary, this study reports a novel mechanism by which the natural sesquiterpene BrA inhibits BC growth, namely by inducing mitochondrial dysfunction and ER stress through WWP2-mediated KLF5 degradation. Our findings provide complementary strategies for selectively destabilizing KLF5 in a context-de-

pendent manner by targeting different E3 ubiquitin ligases, including WWP1, FBXW7, NEDD4L, EFP, and now WWP2. Future studies should focus on elucidating the structural basis of the BrA-KLF5-WWP2 interaction, evaluating its therapeutic relevance *in vivo*, and exploring combination strategies with other metabolic or stress pathway inhibitors. Such approaches may pave the way for developing novel KLF5-targeted therapies in BC and beyond.

Funding

This work was supported by the National Natural Science Foundation of China (Nos. 82473118, and 82372681), the Hubei Provincial Natural Science Foundation (Nos. 2026AFC0253, 2026AFC0257, and 2026AFC0263), the Scientific Research Plan of Department of Education of Hubei Province (No. T2024017), and the National Training Program of Innovation and Entrepreneurship for Undergraduates (No. S202510929021).

Data availability

All data were generated in-house, and no paper mill was used. All authors agree to be accountable for all aspects of work ensuring integrity and accuracy.

Declaration of competing interest

The authors declare no competing interests.

Acknowledgements

We thank Dr. Haitao Zhang from Sir Run Run Shaw Hospital, Zhejiang University School of Medicine, as well as Qingqing Yu, Liting Yang, and Fangzhou Li at the Biomedical Research Institute, Hubei University of Medicine, for their technical support.

References

1 Bray F, Laversanne M, Sung H, et al. Global cancer statistics 2022: GLOBOCAN estimates of incidence and mortality worldwide for 36 cancers in 185 countries. *CA Cancer J Clin*. 2024;74(3):229-263. https://doi.org/10.3322/caac.21834.

2 Yang R, Li Y, Wang H, et al. Therapeutic progress and challenges for triple negative breast cancer: targeted therapy and immunotherapy. *Mol Biomed*. 2022;3(1):8. https://doi.org/10.1186/s43556-022-00071-6.

3 Yuce K, Ozkan AI. The kruppel-like factor (KLF) family, diseases, and physiological events. *Gene*. 2024;895:148027. https://doi.org/10.1016/j.gene.2023.148027.

4 Gao Y, Ding Y, Chen H, et al. Targeting Krüppel-like factor 5 (KLF5) for cancer therapy. *Curr Top Med Chem*. 2015;15(8):699-713. https://doi.org/10.2174/1568026615666150302105052.

5 Yang S, Feng T, Li H. KLF5, a novel therapeutic target in squamous cell carcinoma. *DNA Cell Biol*. 2021;40(12):1503-1512. https://doi.org/10.1089/dna.2021.0674.

6 Ekstrom TL, Dai Z, Thiel J, et al. KLF5 controls subtype-independent highly interactive enhancers in pancreatic cancer to regulate cell survival. *Sci Adv*. 2026;12(12):eaea2106. https://doi.org/10.1126/sciadv.aea2106.

7 Zeng J, Li Q, Zhang J, et al. KLF5 activation promotes malignant transformation to drive development of lung squamous cell carcinoma. *Cancer Res*. 2026;86(7):1622-1638. https://doi.org/10.1158/0008-5472.CAN-25-2139.

8 Luo Y, Chen C. The roles and regulation of the KLF5 transcription factor in cancers. *Cancer Sci*. 2021;112(6):2097-2117. https://doi.org/10.1111/cas.14910.

9 Tang Y, Liu R, Zhu J, et al. Positive feedback regulation between KLF5 and XPO1 promotes cell cycle progression of basal like breast cancer. *Adv Sci (Weinh)*. 2025;12(16):e2412096. https://doi.org/10.1002/advs.202412096.

10 Li J, Liang Y, Zhou S, et al. UCHL1 contributes to insensitivity to endocrine therapy in triple-negative breast cancer by deubiquitinating and stabilizing KLF5. *Breast Cancer Res*. 2024;26(1):44. https://doi.org/10.1186/s13058-024-01800-1.

11 Xie B, Wang M, Xiao Y, et al. Tryptophan metabolic gatekeeping in epithelial repair: GPR35-KLF5 circuitry decodes mucosal damage signals for repair programming. *Cell Death Dis*. 2026;17(1):25. https://doi.org/10.1038/s41419-025-08237-0.

12 Zhang X, Liu F, Wang Q, et al. Overexpressed microRNA-506 and microRNA-124 alleviate H_2O_2-induced human cardiomyocyte dysfunction by targeting krüppel-like factor 4/5. *Mol Med Rep*. 2017;16(4):5363-5369. https://doi.org/10.3892/mmr.2017.7243.

13 Li LY, Yang Q, Jiang YY, et al. Interplay and cooperation between SREBF1 and master transcription factors regulate lipid metabolism and tumor-promoting pathways in squamous cancer. *Nat Commun*. 2021;12(1):4362. https://doi.org/10.1038/s41467-021-24656-x.

14 Zhang Y, Chen JC, Zheng JH, et al. Pterosin B improves cognitive dysfunction by promoting microglia M1/M2 polarization through inhibiting Klf5/Parp14 pathway. *Phytomedicine*. 2024;135:156152. https://doi.org/10.1016/j.phymed.2024.156152.

15 Ma D, Zheng B, Liu HL, et al. Klf5 down-regulation induces vascular senescence through eIF5a depletion and mitochondrial fission. *PLoS Biol*. 2020;18(8):e3000808. https://doi.org/10.1371/journal.pbio.3000808.

16 Gao L, Yang X, Li Y, et al. Curcumol inhibits KLF5-dependent angiogenesis by blocking the ROS/ERK signaling in liver sinusoidal endothelial cells. *Life Sci*. 2021;264:118696. https://doi.org/10.1016/j.lfs.2020.118696.

17 Ma L, Lin C, Xiao Z, et al. Acetylated KLF5 inhibits LACTB transcription, mediates mitochondrial dynamics, and regulates colorectal cancer cell stemness and differentiation. *Int J Biol Macromol*. 2025;333(Pt 2):148905. https://doi.org/10.1016/j.ijbiomac.2025.148905.

18 Deng J, Wang D, Jiang K, et al. Targeting PDK4 to mitigate osimertinib-induced cardiotoxicity: insights into mitochondria-endoplasmic reticulum crosstalk and necroptosis. *Free Radic Biol Med*. 2025;240:267-283. https://doi.org/10.1016/j.freeradbiomed.2025.08.017.

19 Liu Y, Mao ZH, Huang J, et al. Mitochondria-associated endoplasmic reticulum membranes in human health and diseases. *MedComm (2020)*. 2025;6(7):e70259. https://doi.org/10.1002/mco2.70259.

20 Alizade A, Evyapan G, Celik IS, et al. Metformin induces mitochondria-mediated and endoplasmic reticulum stress-mediated apoptosis and inhibits angiogenesis-related gene expression in breast cancer cells *via* targeting VEGF-A/VEGFR2/NRP1. *Croat Med J*. 2025;66(2):115-124. https://doi.org/10.3325/cmj.2025.66.115.

21 Chen C, Sun X, Ran Q, et al. Ubiquitin-proteasome degradation of KLF5 transcription factor in cancer and untransformed epithelial cells. *Oncogene*. 2005;24(20):3319-3327. https://doi.org/10.1038/sj.onc.1208497.

22 Wang TT, Zhang LL, Li FB, et al. LN-439A, a novel BAP1 inhibitor, suppresses the growth of basal-like breast cancer by degrading KLF5. *Acta Pharmacol Sin*. 2025;46(3):715-727. https://doi.org/10.1038/s41401-024-01361-1.

23 Zhao D, Zhi X, Zhou Z, et al. TAZ antagonizes the WWP1-mediated KLF5 degradation and promotes breast cell proliferation and tumorigenesis. *Carcinogenesis*. 2012;33(1):59-67. https://doi.org/10.1093/carcin/bgr242.

24 Shi P, Liu W, Tala, et al. Metformin suppresses triple-negative breast cancer stem cells by targeting KLF5 for degradation. *Cell Discov*. 2017;3:17010. https://doi.org/10.1038/celldisc.2017.10.

25 Du JX, Hagos EG, Nandan MO, et al. The E3 ubiquitin ligase SMAD ubiquitination regulatory factor 2 negatively regulates Krüppel-like factor 5 protein. *J Biol Chem*. 2011;286(46):40354-40364. https://doi.org/10.1074/jbc.M111.258707.

26 Zhao KW, Sikriwal D, Dong X, et al. Oestrogen causes degradation of KLF5 by inducing the E3 ubiquitin ligase EFP in ER-positive breast cancer cells. *Biochem J*. 2011;437(2):323-333. https://doi.org/10.1042/BJ20101388.

27 Wan F, Qian C, Liu X, et al. Sculponeatin A induces mitochondrial dysfunction in non-small cell lung cancer through WWP2-mediated degradation of mitochondrial STAT3. *Br J Pharmacol*. 2025;182(12):2662-2681. https://doi.org/10.1111/bph.17460.

28 Zhang Z, Lu YX, Liu F, et al. lncRNA BREA2 promotes metastasis by disrupting the WWP2-mediated ubiquitination of Notch1. *Proc Natl Acad Sci U S A*. 2023;120(8):e2206694120. https://doi.org/10.1073/pnas.2206694120.

29 Chan CO, Xie XJ, Wan SW, et al. Qualitative and quantitative analysis of sesquiterpene lactones in *Centipeda minima* by UPLC-Orbitrap-MS & UPLC-QQQ-MS. *J Pharm Biomed Anal*. 2019;174:360-366. https://doi.org/10.1016/j.jpba.2019.05.067.

30 Liu YQ, Zhou GB. Promising anticancer activities and mechanisms of action of active compounds from the medicinal herb *Centipeda minima* (L.) A. Braun & Asch. *Phytomedicine*. 2022;106:154397. https://doi.org/10.1016/j.phymed.2022.154397.

31 Qu Z, Lin Y, Mok DK, et al. Brevilin A, a natural sesquiterpene lactone inhibited the growth of triple-negative breast cancer cells *via* Akt/mTOR and STAT3 signaling pathways. *Onco Targets Ther*. 2020;13:5363-5373. https://doi.org/10.2147/OTT.S256833.

32 Saleem MZ, Nisar MA, Alshwmi M, et al. Brevilin A inhibits STAT3 signaling and induces ROS-dependent apoptosis, mitochondrial stress and endoplasmic reticulum stress in MCF-7 breast cancer cells. *Onco Targets Ther*. 2020;13:435-450. https://doi.org/10.2147/OTT.S228702.

33 Xiang Y, Wan F, Ren Y, et al. Polyphyllin VII induces autophagy-dependent ferroptosis in human gastric cancer through targeting T-lymphokine-activated killer cell-originated protein kinase. *Phytotherapy Research*. 2023;

37(12):5803-5820. https://doi.org/10.1002/ptr.7986.
34 Peng P, Ren Y, Wan F, et al. Sculponeatin A promotes the ETS1-SYVN1 interaction to induce SLC7A11/xCT-dependent ferroptosis in breast cancer. *Phytomedicine*. 2023;117:154921. https://doi.org/10.1016/j.phymed.2023.154921.
35 Ren Y, Chen J, Zhan X, et al. Liquid-liquid phase separation of GPS2-LATS1 promotes colorectal cancer progression by reprogramming lipid metabolism . *Oncogene*. 2025;44(39):3741-3754. https://doi.org/10.1038/s41388-025-03498-7.
36 Si Y, Ou H, Jin X, et al. G protein pathway suppressor 2 suppresses aerobic glycolysis through RACK1-mediated HIF-1α degradation in breast cancer. *Free Radic Biol Med*. 2024;222:478-492. https://doi.org/10.1016/j.freeradbiomed.2024.06.021.
37 Xiang YC, Shen J, Si Y, et al. Paris saponin VII, a direct activator of AMPK, induces autophagy and exhibits therapeutic potential in non-small-cell lung cancer. *Chin J Nat Med*. 2021;19(3):195-204. https://doi.org/10.1016/S1875-5364(21)60021-3.
38 Wu Y, Si Y, Xiang Y, et al. Polyphyllin I activates AMPK to suppress the growth of non-small-cell lung cancer *via* induction of autophagy. *Arch Biochem Biophys*. 2020;687:108285. https://doi.org/10.1016/j.abb.2020.108285.
39 Xiang YC, Peng P, Liu XW, et al. Paris saponin VII, a Hippo pathway activator, induces autophagy and exhibits therapeutic potential against human breast cancer cells. *Acta Pharmacol Sin*. 2022;43(6):1568-1580. https://doi.org/10.1038/s41401-021-00755-9.
40 Xu J, Chen Y, Yang R, et al. Cucurbitacin B inhibits gastric cancer progression by suppressing STAT3 activity. *Arch Biochem Biophys*. 2020;684:108314. https://doi.org/10.1016/j.abb.2020.108314.
41 Si Y, Zhang H, Peng P, et al. G protein pathway suppressor 2 suppresses gastric cancer by destabilizing epidermal growth factor receptor. *Cancer Sci*. 2021;112(12):4867-4882. https://doi.org/10.1111/cas.15151.
42 Ren Y, Wu H, Tan M, et al. Acetylation of MOB1 mediates polyphyllin II-reduced lysosome biogenesis in breast cancer by promoting the cytoplasmic retention of the YAP/TFEB coactivator complex. *Phytomedicine*. 2024;122:155152. https://doi.org/10.1016/j.phymed.2023.155152.
43 Dittmar G, Winklhofer KF. Linear ubiquitin chains: cellular functions and strategies for detection and quantification. *Front Chem*. 2019;7:915. https://doi.org/10.3389/fchem.2019.00915.
44 Ziegler DV, Parashar K, Leal-Esteban L, et al. CDK4 inactivation inhibits apoptosis *via* mitochondria-ER contact remodeling in triple-negative breast cancer. *Nat Commun*. 2025;16(1):541. https://doi.org/10.1038/s41467-024-55605-z.
45 Sassano ML, Tyurina YY, Diokmetzidou A, et al. Endoplasmic reticulum-mitochondria contacts are prime hotspots of phospholipid peroxidation driving ferroptosis. *Nat Cell Biol*. 2025;27(6):902-917. https://doi.org/10.1038/s41556-025-01668-z.
46 Urra H, Dufey E, Avril T, et al. Endoplasmic reticulum stress and the hallmarks of cancer. *Trends Cancer*. 2016;2(5):252-262. https://doi.org/10.1016/j.trecan.2016.03.007.
47 Chen J, Ying K, Sun J, et al. NEDD4L affects KLF5 stability through ubiquitination to control ferroptosis and radiotherapy resistance in oesophageal squamous cell carcinoma. *J Cell Mol Med*. 2024;28(18):e70062. https://doi.org/10.1111/jcmm.70062.